



Conference Paper

The Application of Scanning Contact Potentiometry Method and Diffraction of Thermal Neutrons at Physico-Mechanical Tests of Materials

A. A. Abu Ghazal¹, G. D. Bokuchava², I. V. Papushkin², V. I. Surin¹, and E. A. Shef¹¹National Research Nuclear University MEPhI (Moscow Engineering Physics Institute), Kashirskoe shosse 31, Moscow, 115409, Russia²Frank Laboratory of Neutron Physics, Joint Institute for Nuclear Research, Dubna, Russia

Abstract

The results of physical and mechanical tests on the tensile strength of austenitic steel 12X18H10T, in the stress range from 100 MPa to the maximum value of 700 MPa, at which the sample was destroyed, are presented. Structural changes were registered synchronously by two methods: the method of scanning contact potentiometry and the method of diffraction of thermal neutrons. At loads above 650 MPa, the α -martensite phase was found in the austenite matrix, as well as the appearance of diffraction peaks characteristic of a cubic martensitic BCC lattice was observed in neutron spectra. On the potentiograms, this process corresponds to the appearance of local regions in which high values of electric potential gradients were observed. This is the case of discovery of the fatigue nucleus cracks in the tensile testing of steel ЭИ847 by the method of scanning contact potentiometry.

Keywords: method of scanning contact potentiometry, the method of thermal neutron diffraction, martensitic transformation in austenitic steel

1. INTRODUCTION

Diagnostics of materials with physical and mechanical testing are established and relate to the solution of some complex tasks, which are detection and identification of structural defects at different stages of testing to determine the strength properties of the material and prediction of its behavior. Signals of electro-physical diagnostic contain a significant amount of useful information about physical processes, changes in the structure of the material and the kinetics of destruction, etc. The process of deformation accumulation develops in stages; each stage is controlled by certain mechanisms, and gives its contribution to the overall process. The work on the methods of

Corresponding Author:

A. A. Abu Ghazal

gazal.ayman@yandex.ru

Received: 23 December 2017

Accepted: 15 January 2018

Published: 21 February 2018

Publishing services provided by
Knowledge E

© A. A. Abu Ghazal et al. This article is distributed under the terms of the [Creative Commons Attribution License](#), which permits unrestricted use and redistribution provided that the original author and source are credited.

Selection and Peer-review under the responsibility of the AtomFuture Conference Committee.



processing the electro-physical signals diagnostics aims to achieve reliable results on identification of deformation stages and damage accumulation of materials that leads to destruction, for a clearer understanding of the processes and possibilities of external influence that affect their development.

The use of the method of scanning contact potentiometry (SCP) opens up opportunities to study the distribution of surface stresses, deformations, mechanisms of plastic deformation, stages of development of internal defects until destruction and other physical processes in real time. Informative electric signal is formed on the contact of the transducer with the test object under load; the mechanical contact surface is a sensitive element of electro-physical transducer. The number of contact spots of the Converter is determined by the intensity of contact interaction in the contact zone and the processes occurring in this area, as well as substantially independent of changes in waviness and roughness parameters.

Sensors of contact potentiometry method have several advantages compared to measuring devices of other NDT methods. The main of these advantages are: low weight and small dimensions of sensitive elements; due to the spots small linear dimensions formed of micro-constrictions, high reliability and reproducibility of measurements, high noise immunity and low noise level. There are no high-current circuits and heated areas in sensor designs, therefore measuring systems are characterized by high fire safety. It should be also noted the low power level of the useful signal and the absence of sparking in mechanical contacts. The SCP method provides the possibility of multi-point and distributed measurements, including the use of time-frequency multiplexing of sensitive elements located on different portions of the test object. For handling, the flow of incoming information is used to code a temporal and spectral analysis.

Purpose of this work: joint the applications of SCP and diffraction thermal neutrons (Fourier stress-diffractometer FSD) methods in the testing of austenitic steel 12X18H10T for destruction at pulsed fast reactor IBR-2 in the FLNP JINR (Dubna, Russia).

2. MATERIALS AND METHODS OF RESEARCH

2.1. Method of scanning contact potentiometry

Potentiometric measurements were performed using a desktop device called Spectroelph-FRR, intended for spectral analysis of electrical signals [1]. The device works in conjunction with a hardware-software system mobile diagnostic system,

TABLE 1: Work parameters of the LM-29 stress rig.

Maximal load	±29 kN
Temperature range	Up to 800 °C
Sample dimensions	30-100 mm
Sample elongation measurement	Mechanical extensometer
Control	PC (Windows/VME)

2.2. Method of Thermal Neutrons Diffraction

The diffraction of neutrons is in many respects similar to the scattering of X-rays. The velocity of thermal neutrons is sufficiently small, and the energy spectrum has a continuous (Maxwellian) character, which allows the analysis of the neutron energy in time-of-flight (TOF method) when the experiment is performed on a pulsed source. Depending on the neutron wavelength, the position of the diffraction peaks on the time scale is defined as:

$$t = (L/v) = (\lambda m L / h) = (2m L d_{hkl}) \sin(\theta / h), \quad (1)$$

Where;

L : total flight distance from neutron source to detector,

v : neutron velocity,

λ : neutron wavelength,

m : neutron mass,

h : Planck's constant,

d_{hkl} : the interplanar distance for crystal planes with Miller indices (hkl) ,

θ : Bragg angle.

The internal stresses existing in the material cause the corresponding deformation of the crystal lattice, which in turn is expressed in the shift of the Bragg peaks in the diffraction spectrum. When using a TOF diffractometer on a pulsed neutron source, the crystal lattice strain is determined by the relative change in the neutron time of flight $\Delta t/t$:

$$\varepsilon_{hkl} = (d_{hkl} - d_{hkl}^0) / d_{hkl}^0 = \Delta t / t, \quad (2)$$

Where;

d_{hkl}, d_{hkl}^0 : Interplanar distances for the deformed and non-deformed lattices respectively,

t : neutron time of flight.

Further, from the measured residual strains, we can determine the components of the residual stress tensor:

$$\sigma_{ii} = \frac{E}{1 + \nu} \left(\epsilon_{ii} + \frac{\nu}{1 - 2\nu} (\epsilon_X + \epsilon_Y + \epsilon_Z) \right), \quad (3)$$

Where;

$ii = X, Y, Z,$

$\sigma_{ii}, \epsilon_{ii}$: components of stress and strain tensors, respectively,

E : the Young's modulus,

ν : Poisson's ratio.

The essence of the diffraction method for studying stresses in the standard layout of the experiment consists in the formation of incident and scattered neutron beams by means of diaphragms or radial collimators, and in the selection of a small scattering volume in the sample as shown in Fig. 2. In this case, the relative displacements of the diffraction peaks from the positions determined by the parameters of the unit cell of the undeformed material are measured, which, according to formula (2), is recalculated in the strain in a direction parallel to the neutron scattering vector \mathbf{Q} .

In addition, very useful information is the analysis of the shape (in the simplest case of the width) of the diffraction peaks, which makes it possible to estimate the magnitude of crystal lattice distortions within individual grains (microstrains) and the sizes of coherent scattering domains. It is particularly convenient to do this on a TOF diffractometer based on the functional dependence of the peaks width of the interplanar distance [4]:

$$W^2 = C_1 + C_2 d^2 + C_3 d^2 + C_4 d^4, \quad (4)$$

Where;

W : peak width,

C_1 and C_2 : constants for determining the resolution function of the diffractometer and known from measurements with a standard sample,

$C_3 = (\Delta a/a)^2$: dispersion of the unit cell parameter (microstrain),

C_4 : constant related to the size of the crystallites.

In Frank Laboratory of Neutron Physics of the Joint of Institute for Nuclear Research (Dubna, Russia) at a long pulse neutron source - IBR-2 reactor, a specialized neutron Fourier stress diffractometer FSD was designed to investigate internal stresses in bulk industrial samples and thermo-mechanical properties of structural materials.

A unique method of neutron correlation time-of-flight diffractometry [5] – the use of a fast Fourier chopper for primary neutron beam intensity modulation and the RTOF method for data acquisition – makes it possible to obtain on FSD the diffraction spectra with the required high resolution ($\Delta d/d \approx 2 \times 10^{-3}$ at a scattering angle of $2\theta = 140^\circ$ and $\Delta d/d \approx 4 \times 10^{-3}$ at scattering angles $2\theta = \pm 90^\circ$) over a wide range of interplanar distances, which provides the necessary accuracy of registration a small displacements of diffraction peaks and their broadening. The FSD experimental equipment includes a precise Huber goniometer with a carrying capacity up to 300 kg, a high-temperature mirror furnace that allows samples to be heated up to 1000 °C, automated diaphragms.

A distinctive feature of the FSD diffractometer is the use of two detectors at scattering angles $\pm 90^\circ$ with large solid angles (~ 0.1 sr each) and high resolution. A system of radial collimators with a wide aperture installed in front of the 90° -detectors provides a minimum scattering volume of $2 \times 2 \times 2$ mm in the sample, in which the crystal lattice strain is measured (see Fig. 2). This makes it possible to substantially increase the luminosity of the experiment due to the full use of the detector system and to effectively carry out experiments to study the residual stresses in thick samples (up to 30 mm).

One of the advantages of neutron TOF diffraction is a wide interval of interplanar distances, which allows one to register a set of diffraction peaks simultaneously. This makes it possible to study the behavior of polycrystalline materials with a rather complex structure, including multiphase ones, in fixed geometry under various external conditions [6].

To study the behavior of structural materials under external load and high temperature directly in the neutron beam on the FSD *in situ*, the mechanical type LM-29 testing machine is used, which allows the sample to be subjected to uniaxial tension or compression up to 29 kN and heating up to 800 °C by passing electric current through the sample. The control system allows forming any necessary combination of external load and temperature values on the sample, which significantly expands the range of possible experiments on the diffractometer. As a rule, in similar experiments, detectors at scattering angles $2\theta = \pm 90^\circ$ detect the diffraction spectra at certain values of the load at the sample. At the same time, two independent components of deformation (longitudinal and transverse) are measured simultaneously in the direction of the external load, parallel and perpendicular to the neutron scattering vector \mathbf{Q} .

3. EXPERIMENTAL RESULTS AND DISCUSSION

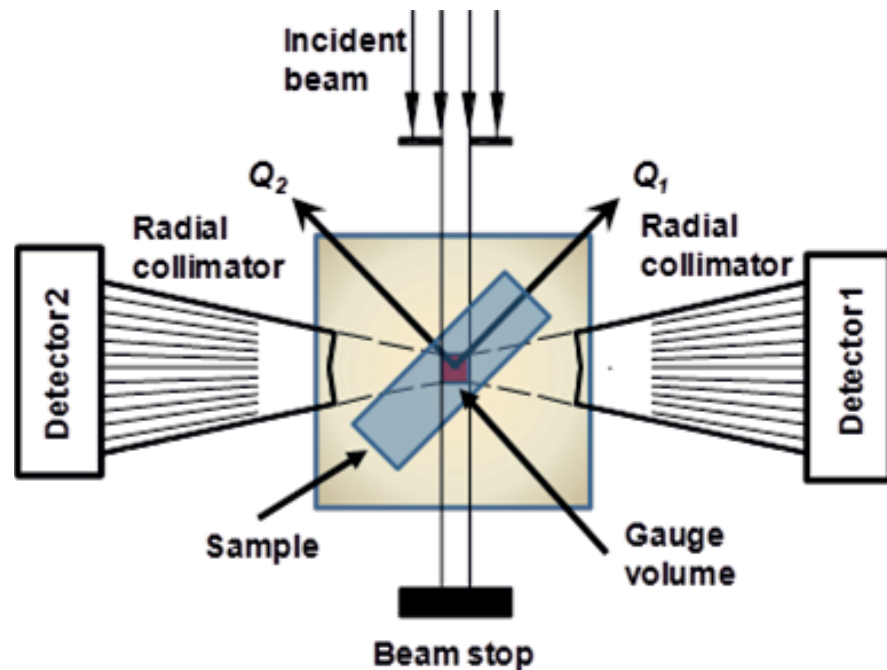


Figure 2: Experiment on the study of residual stresses in a bulk sample by neutron diffraction.

3.1. Results of Scanning Contact Potentiometry method

Registration of electric potential difference on the sample surface and analysis of diagnostic information produced on the hardware-software complex "ElphysLAB-IDS" mobile information and diagnostic system (IDS). Developed a software package that is included in the calculation is a software module IDS allows the user to remotely provide processing of incoming information to form a database and make the necessary calculations for the visualization of the obtained results and patient diagnosis. When the load was increased, a color gamut of changes in the surface potential was observed on the potentiogram (Figure 3), caused by the influence of mechanical stresses and the formation of dynamic roughness. This was particularly noticeable under loads exceeding the yield strength. For the analysis of the measurement results using PAD with broad functionality.

In upper figure (Figure 3) at 400 MPa presented the process of concentration of internal stresses at three locations on the sample (red-yellow tones). With the left and right sides of the specimen, the stress concentration occurs near the throat, in the region of the transition from the diameter of the working part of the specimen to the diameter of the threaded part (Figure 2) in the center – where there is the most effective stress. In the process of plastic flow zones are being established localization of macro-deformation that is clearly visible at a load of 600, and especially at 650 MPa.

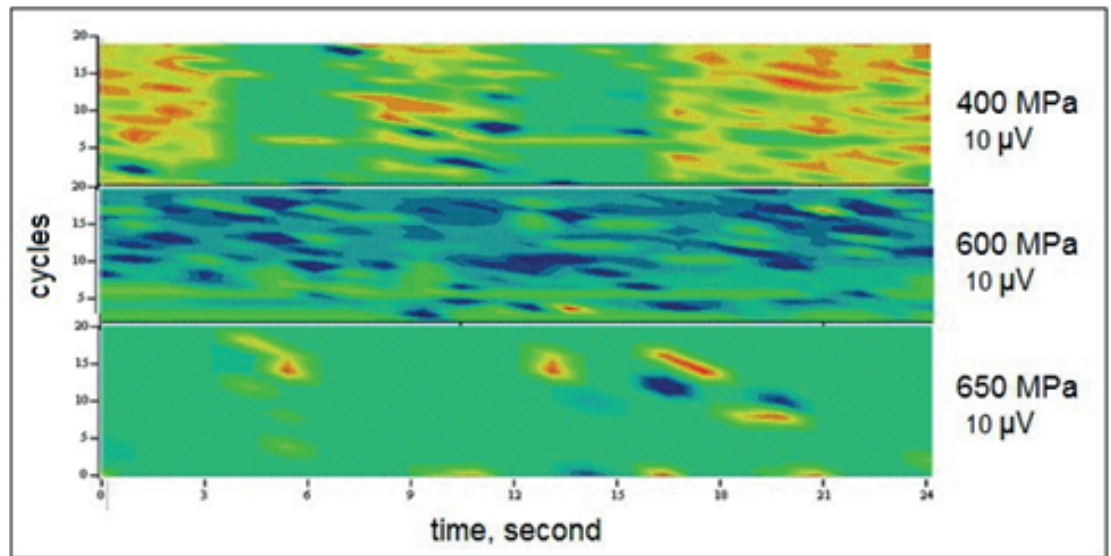


Figure 3: Potentiograph the surface of the sample, pre-tested, with loads of 400, 600 and 650 MPa. On the left vertical scale shows the number of measurement cycles, to the right is the applied stress and the value of SLS.

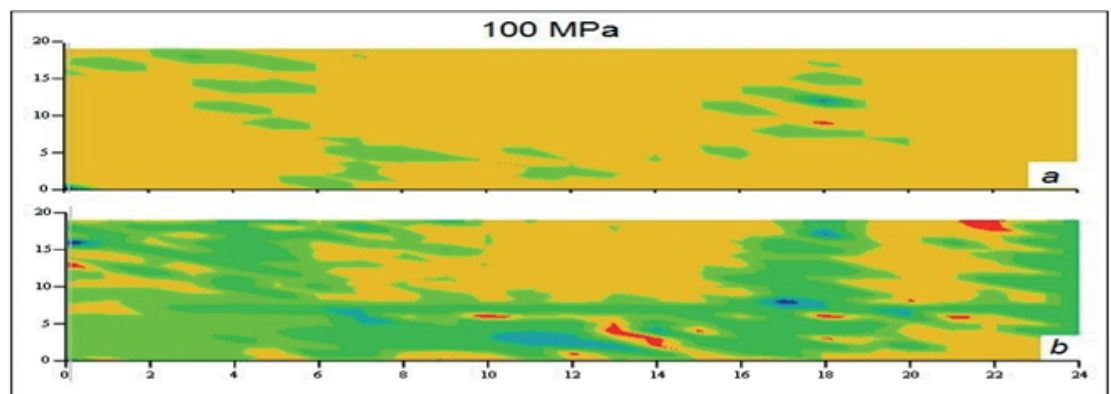


Figure 4: Potentiograph the surface of the sample № 1 with a load of 100 MPa. SLS is equal to (a): 10^{-1} V and (b): $2 \cdot 10^{-5}$ V.

In these zones, at this and higher loads, leads to the formation of a local constriction or neck.

The high resolution measurement (SLS~10 microvolts), enable you to define a local region with relatively high values of internal stresses (stresses of the III kind) in the region of the elastic and quasi-elastic deformation (Figure 4 b and Figure 5 b).

At a stress of 200 MPa it is possible to see the trend of concentration of internal stresses at three locations on the sample (Figure 5.b), the same as in Figure 3. At higher loads the color pattern is undergoing significant changes at the level of microplastic deformation (Figure 6. b) high stress start mainly concentrate on the right part of the specimen, spreading to the middle and beyond. It should be noted that a small linear region with a high value of the potential at the left side of the sample (Figure 6.a and

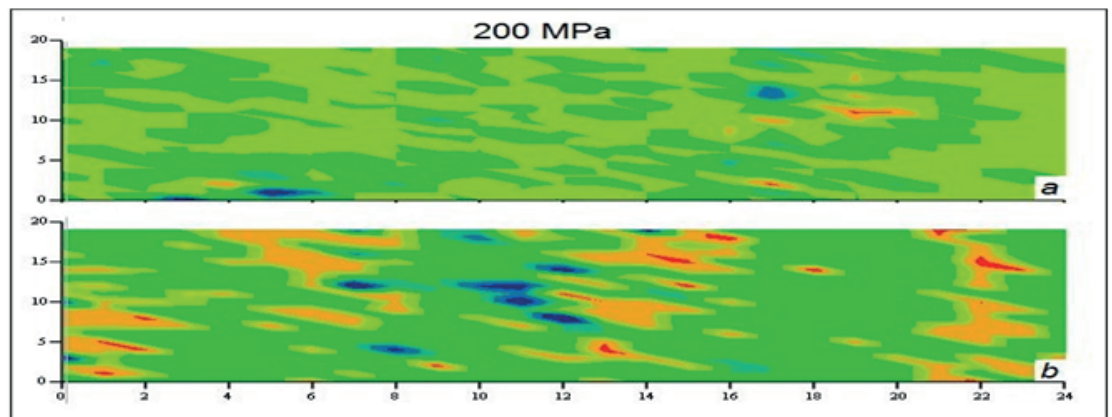


Figure 5: Potentiograph the surface of the sample N° 1 at a load of 200 MPa. SLS is equal to (a): 10^{-1} V and (b) $2 \cdot 10^{-5}$ V.

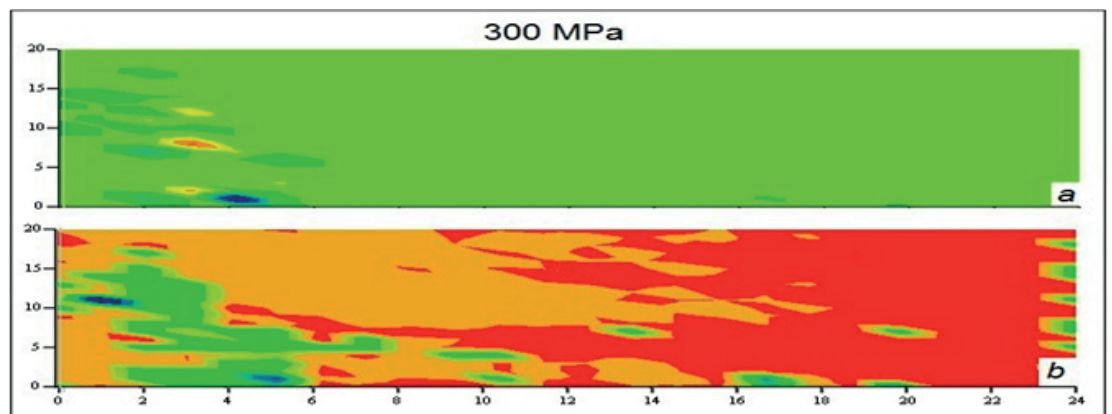


Figure 6: Potentiograph the surface of the sample N° 1 with a load of 300 MPa. SLS is equal to (a): 10^{-1} V and (b): $2 \cdot 10^{-5}$ V.

Figure 7.a) in consequence of not have a noticeable impact on the formation of the neck and disappeared at higher loads.

Joint analysis of the results of the two presented methods suggests that the formation of the phase α' -martensite, apparently, already begun with loads of 400-600 MPa, when potentiograph began to appear alternating local area in the form of multi-colored spots (Figure 7.b, and Figure 8.c) in which the gradients of the electric potential are associated with high rate of change of its polarity. This does not contradict the theory of martensite deformation [7], according to which the role of plastic deformation in shear transformation is varied.

First, it may be associated with a gradual increase in the level of internal stresses before the appearance of martensite stress and overcome the resistance of an accommodation. Secondly, as the load increases, martensite nuclei arise, corresponding to a particular type of defect. In austenitic steels of this class, nuclei are α' -martensite plates with a thickness of 5-7 nm, which appear at the junction of two avalanche

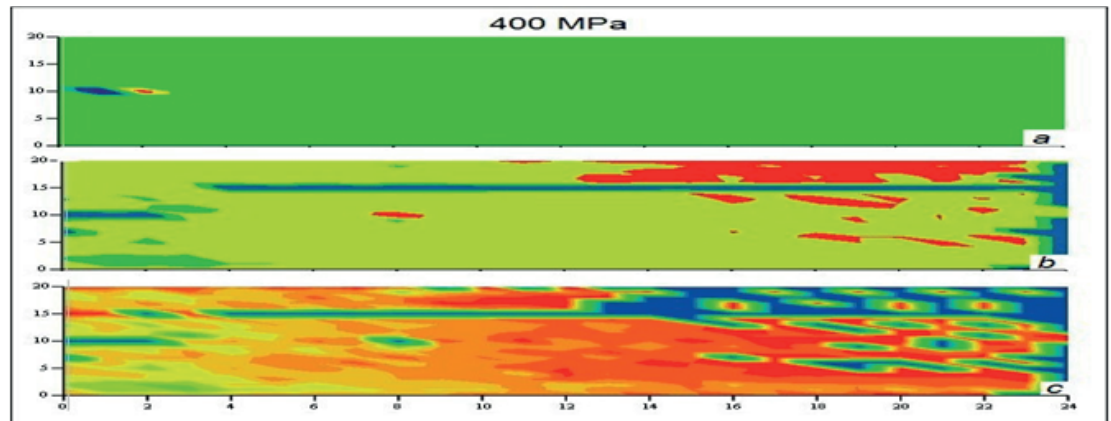


Figure 7: Potentiogram of the surface of sample N°1 at a load of 400 MPa. The SLS is 10^{-1} V (a): $2 \cdot 10^{-5}$ V (b): $1.5 \cdot 10^{-5}$ V (c): 10^{-5} V.

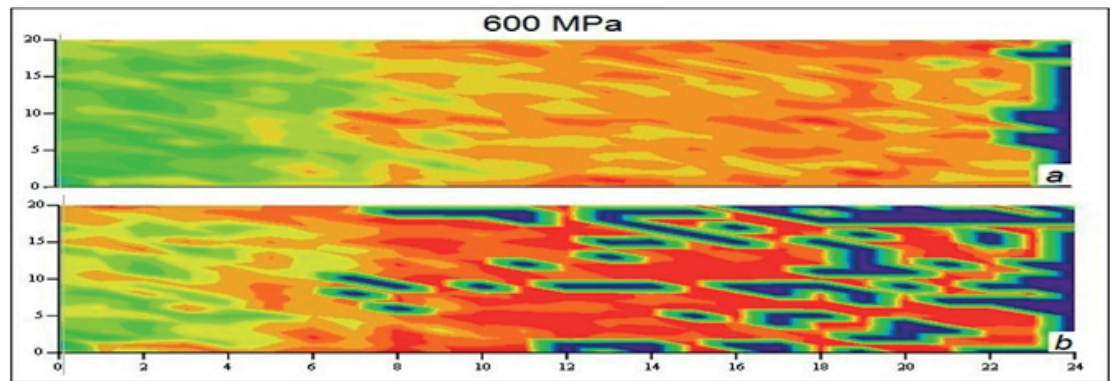


Figure 8: Potentiogram the surface of the sample N°1 at 600 MPa. SLS is equal to (a): 10^{-1} V (b): $1.5 \cdot 10^{-5}$ V.

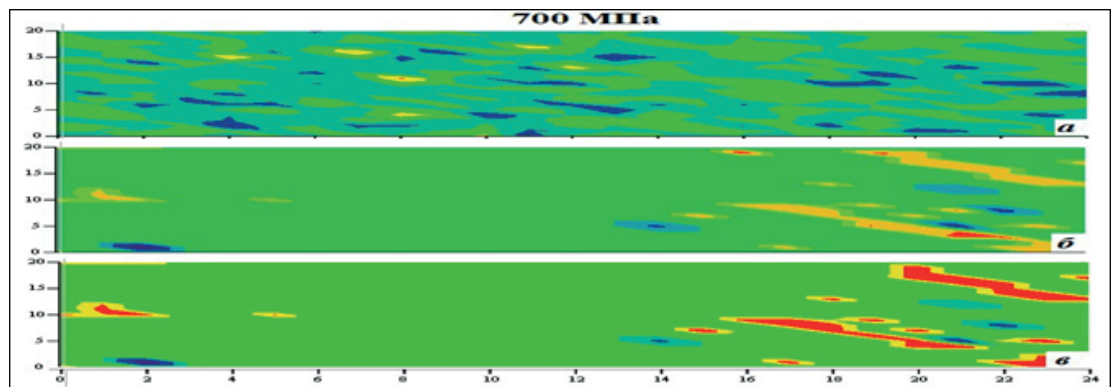


Figure 9: Potentiogram the surface of the sample N°1 at a load of 700 MPa. SLS is equal to (a): 10^{-1} V (b): $2 \cdot 10^{-5}$ V (c): $1.5 \cdot 10^{-5}$ V.

dislocations or when two stacks of stacking faults intersect in the slip band. Thirdly, the medium in which the crystal grows changes, which significantly affects the kinetics of the process. The latter, apparently, has a special influence on the morphology of the electrical double layer, in which the mentioned high-speed inversion of the potential sign occurs.

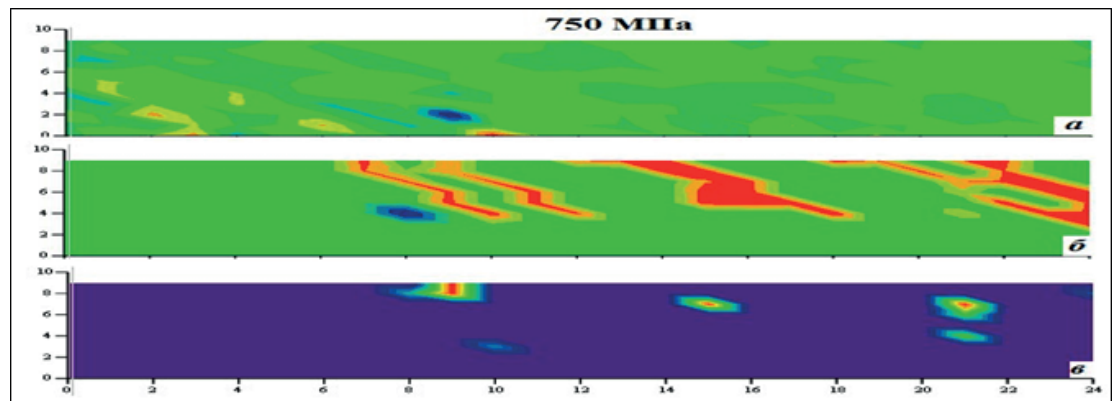


Figure 10: Potentiograph the surface of the sample N^o. at a load of 750 MPa. SLS is equal to (a): 10^{-1} V (b): $2 \cdot 10^{-5}$ V (c): $1 \cdot 10^{-5}$ V.

The beginning and development of the localization process of microdeformation can be observed in the measurements with relatively low values of WM (Figure 8.a, Figure 9.a and Figure 10.a), while the appearance of nuclei of martensite is visible only when the $SLS \leq 20 \mu\text{V}$. In the framework of the mathematical model of the electrical micro contact [8] and models of the deformation activity of metal surfaces [9] this is due to the relatively low amplitude and the energy of the mechanical waves generated by the sources of internal stresses formed around the nuclei of martensite.

Figure 11 shows potentially on the surface of sample N^o2 (with a welded seam in the middle), for SLS $10 \mu\text{V}$ and the five measurement cycles. For loads larger than 100 MPa is a clear border separating two halves of the sample. The welded seam damps external tensile stresses, for this reason, the potential value is lower on the left side of the sample than on the right. The boundary gradually begins to erode under the influence of the resulting martensite, the appearance of which can also be judged by a sharp change in the character of the curves of the deterministic signal component at 600-700 MPa loads (Figure 12).

The regions with a high potential gradient, shown in Figure 10.c, can also be associated with the resulting micronutrient observed during the fatigue tests of ЭИ847 steel [see 9]. The structure of the diagnostic signal was analyzed on different SSS, starting from values of the order of $0.5 \mu\text{V}$. It has been established that the first and second-order voltages (by Davidenkov's criterion) most significantly affect the sign and amplitude of the diagnostic signal, while the low-amplitude component of the signal, which is associated with strains of the third kind, is practically always screened. The potentiograms shown in Figure 13 were constructed by mathematical extrapolation of the results of point-wise scanning along eight measuring tracks to the entire working surface of the sample.

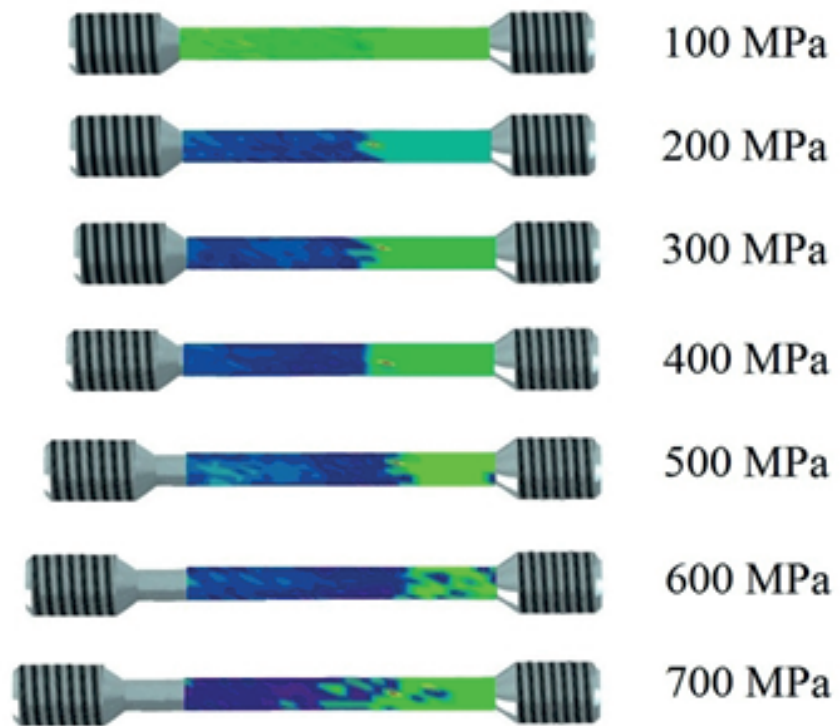


Figure 11: Potentiogram on the surface of sample N° 2 at loads of 100-700 MPa and SLS $1,0 \cdot 10^{-5}$ V.

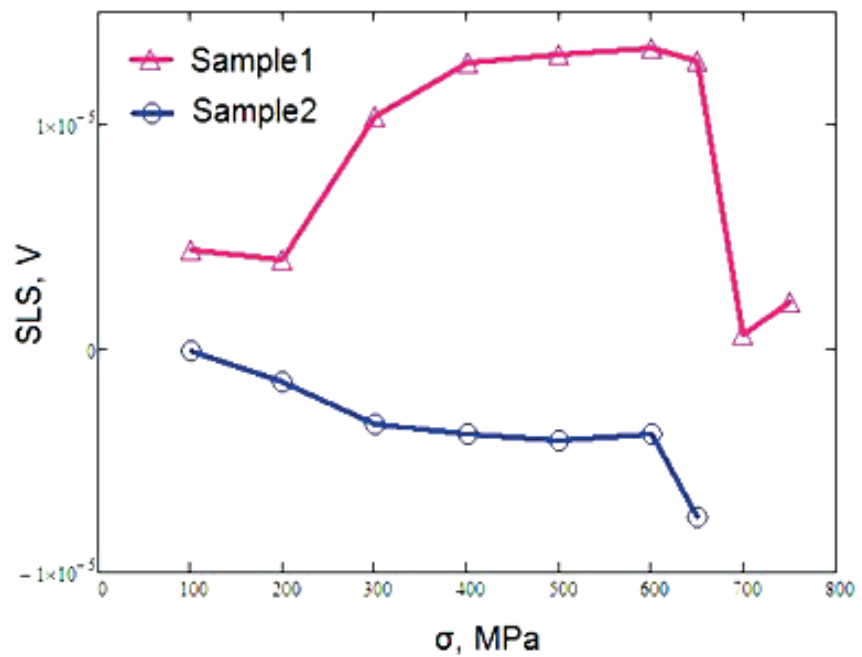


Figure 12: Change in the deterministic component of the diagnostic signal (trend) during testing of sample N° 2 in the range of loads of 100-700 MPa. The stocktickerSLS value corresponds to $2,0 \cdot 10^{-5}$ V.

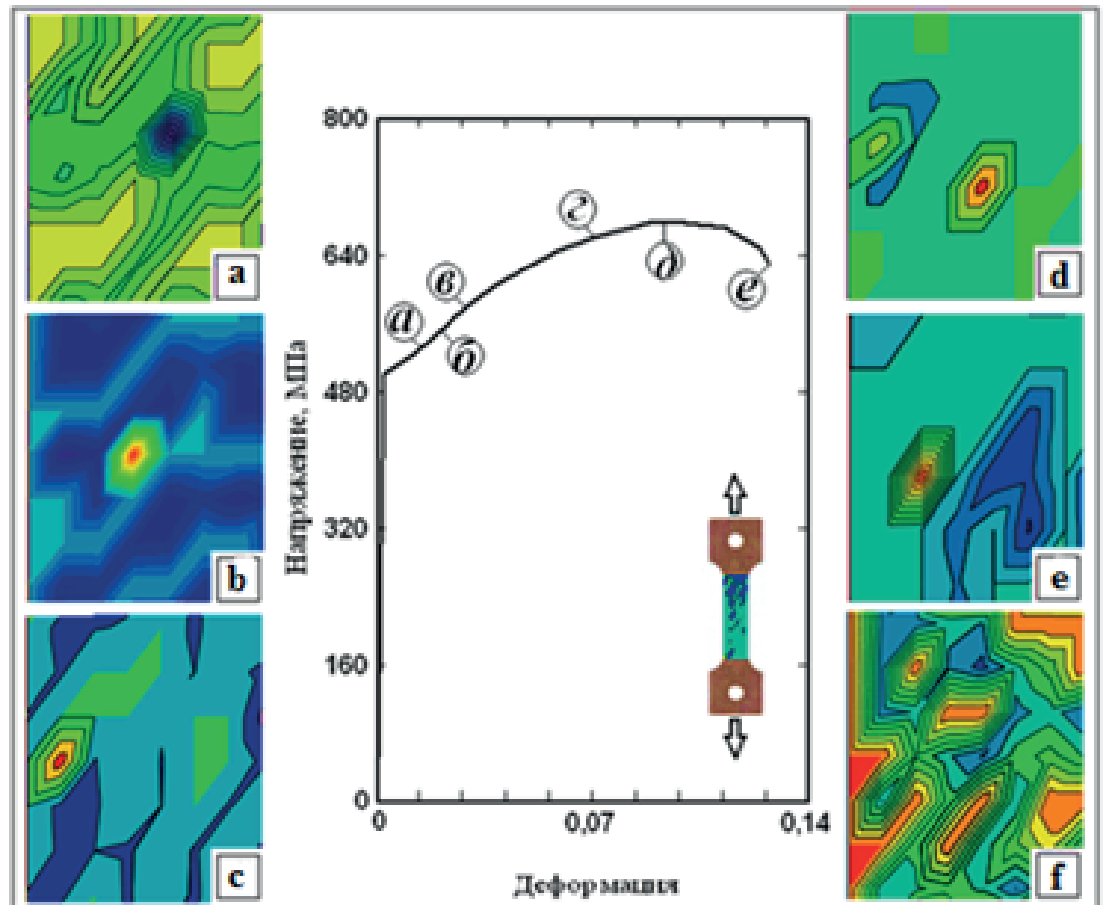


Figure 13: Stress-strain diagram of steel ЭИ847 (center) and fragments of surface potentiograph of stress concentrator, identified as the microscopic crack nucleus in the area of localization of the defect: (a): $\sigma = 525$ MPa, SLS = $2 \cdot 10^{-5}$ V, (b): 550 MPa, SLS = $1.4 \cdot 10^{-5}$ V, (c): 590 MPa, SLS = $1 \cdot 10^{-5}$ V, (d): 650 MPa, SLS = $3,7 \cdot 10^{-4}$ V, (e): 680 MPa, SLS = $2 \cdot 10^{-5}$ V, (f): 630 MPa, SLS = $5 \cdot 10^{-6}$ V (destruction, the central part of the sample).

3.2. The results of neutron diffraction

Neutron diffraction experiments were performed on Fourier stress diffractometer FSD at the IBR-2 pulsed reactor in FLNP JINR (Dubna). During the experiment the investigated 12X18H10T steel samples were subjected to external uniaxial tensile load *in situ* in the neutron beam using the LM-29 testing machine. At the same time, during the neutron experiment, simultaneously with the diffraction spectra, the data of the scanning contact potentiometry were independently recorded. Sample № 1 was subjected to a load in the range from 100 to 700 MPa before the formation of a noticeable (visible) neck in the sample. The last measurement was carried out at a load reduced to 650 MPa in order to avoid the destruction of the sample. Sample № 2 with a welded seam was subjected to a load in the range from 100 to 700 MPa until the sample

was completely destroyed. The last measurement was carried out with the sample completely destroyed (rupture) with the load removed ($\sigma = 0$ MPa).

Diffraction spectra were recorded by detectors at scattering angles $2\theta = \pm 90^\circ$ for each load value on the sample (Figure 14). The measured spectra were processed by profile analysis according to the Rietveld method [10], as a result of which the values of the crystal lattice parameters of the material and the parameters of broadening of the diffraction peaks were obtained. The longitudinal strain (\parallel) was registered by AL detector ($2\theta = +90^\circ$), the perpendicular (\perp) - by AR detector ($2\theta = -90^\circ$). The crystal lattice strain for the austenite phase was calculated as $\varepsilon = (a - a_0)/a_0$, where a and a_0 - the parameters of the crystal lattice of the deformed and undeformed materials, respectively.

The diffraction peaks from the initial austenitic steel corresponded to the cubic FCC lattice (sp. gr. $Fm\bar{3}m$). With the increase in the degree of plastic deformation of the material at loads above 650 MPa, the formation of the α' -martensite phase was detected in an austenite matrix, while the appearance of diffraction peaks characteristic of a cubic martensitic BCC lattice (sp. gr. $Im\bar{3}m$) was observed in neutron spectra (Figure 15). Analysis of the intensities of the diffraction peaks in the spectra showed the presence of a noticeable texture in the initial sample of austenitic steel, and a strong texture is also observed in the martensite formed.

Estimates for the elasticity modulus and Poisson's ratio for the austenitic phase were made from the linear approximation of the $\varepsilon(\sigma)$ dependences in the elastic strain region (up to 500 MPa): $E = 182$ GPa and $\nu = 0.29$ for sample № 1, $E = 195$ GPa and $\nu = 0.30$ for sample № 2 (Figure 16). At loads more than 500 MPa, the deformation of the material was plastic, and there was a noticeable broadening of the diffraction peaks, increasing with an increase in the external load, due to an increase in the dislocation density in the material. From the broadening of the diffraction peaks, the value of the crystal lattice microstrain was estimated as a function of the applied load (Figure 16). At loads in excess of 700 MPa, the formation of a neck on the right side of the specimen was visually observed, which indicates the localization of plastic deformation in this region and the termination of plastic deformation in the remaining volume of the sample.

4. CONCLUSIONS

1. For the first time in comprehensive studies of austenitic steel 12X18H10T, methods of scanning contact potentiometry and diffraction thermal neutrons on Fourier stress

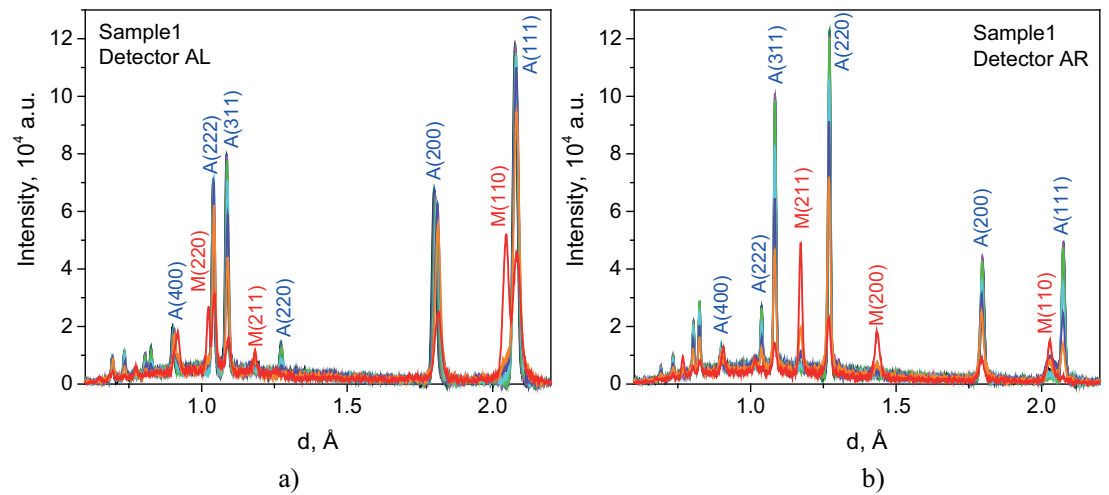


Figure 14: Measured TOF diffraction spectra from sample № 1 for left AL (a) and right AR (b) detectors. The Miller indices for the main austenite and martensite peaks formed as a result of plastic deformation are indicated.

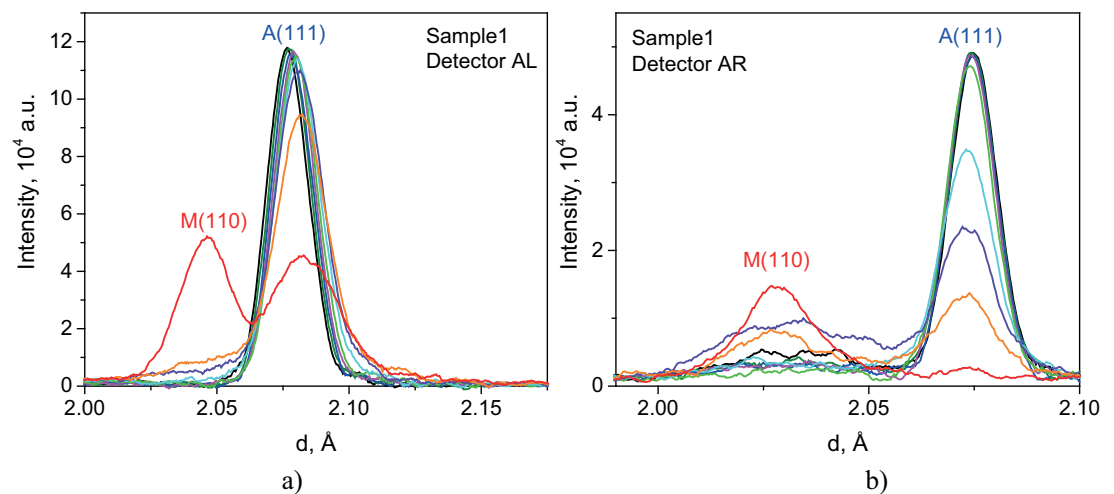


Figure 15: The spectra region from sample № 1 for the left AL (a) and right AR (b) detectors in the region of the austenite (111) and (110) martensite peaks.

diffractometer FSD were tested on a testing machine LM-29 at pulsed fast reactor IBR-2 in FLNP JINR and received unique results.

2. The formation of a phase of α' -martensite was detected by a method of diffraction of thermal neutrons at loads above 650 MPa in an austenite matrix. The presented analysis of the results by two methods makes it possible to estimate the initial stage of the formation of α' -martensite nuclei, which is already observed at 400-600 MPa on potentiograms in the form of alternating local regions in which the electric potential gradients are caused by a high rate of change in its polarity.

3. Linear approximation of the dependences $\epsilon(\sigma)$ in the area of deformation corresponding to stresses up to 500 MPa gives values for the modulus of elasticity and

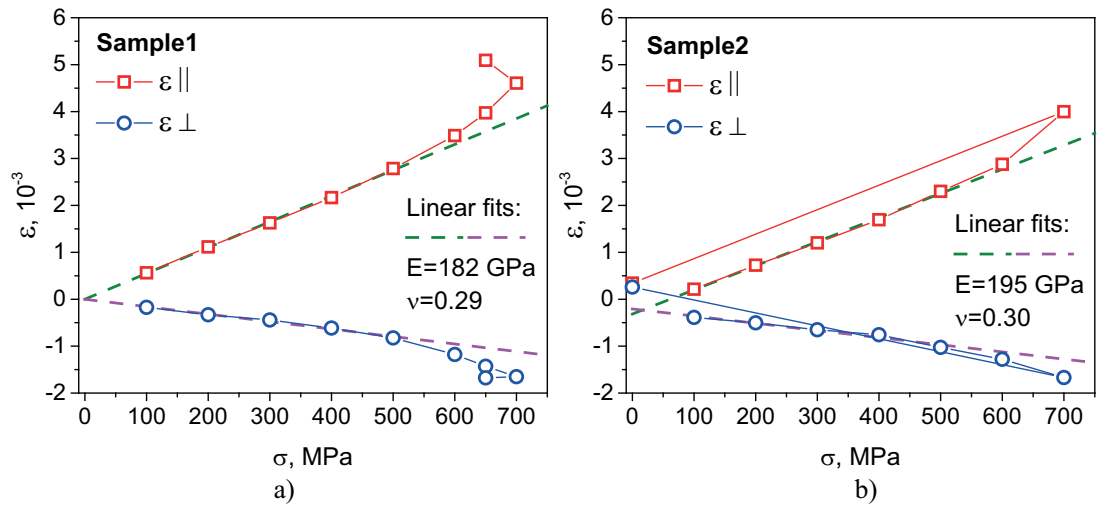


Figure 16: Crystal lattice strain for the austenite phase as a function of the applied load for sample N° 1 (a) and sample N° 2 (b).

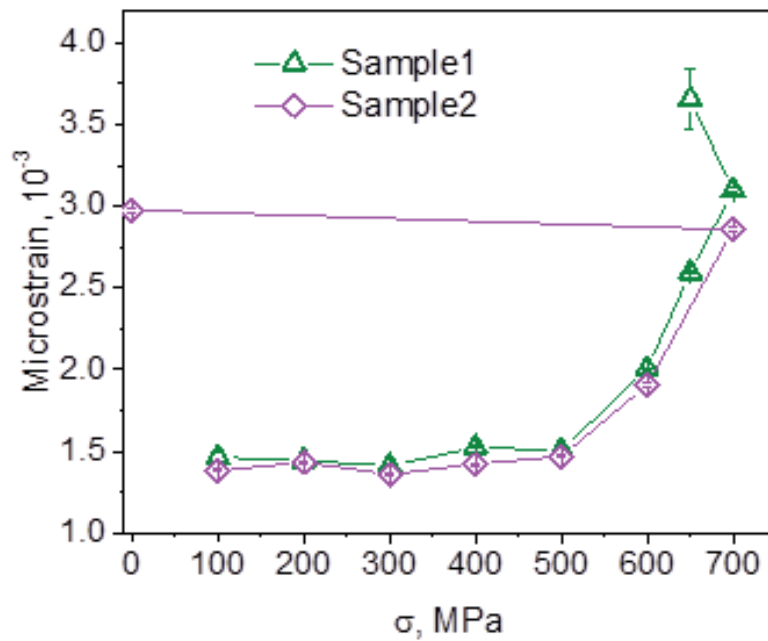


Figure 17: The averaged over all (hkl) crystal lattice microstrain estimated from the broadening of the diffraction peaks, depending on the applied load for both samples. For sample N° 2, the last measured value at $\sigma = 0$ MPa corresponds to the destruction of the sample.

Poisson’s ratio austenitic phase: $E = 182$ GPa and $\nu = 0.29$ for sample N° 1 and $E = 195$ GPa and $\nu = 0.30$ for sample N° 2.

4. Electro-physical measurements conducted on the hardware-software complex “ElphysLAB-IDS” using the desktop device *Spectroelph-FRR*, with a resolution $SLS \leq 10$ μ V help to identify local areas with relatively high values of internal stresses in the region of elastic and quasi-elastic deformation. In the process of plastic flow in the sample volume are formed in the zone of localization of macrodeformation that is

clearly manifested in potentiograph at a stress of 600, and especially at 650 MPa. In one of these areas later formed the neck and there is a destruction of the sample.

5. The beginning and development of the localization process of microdeformation observed in the measurements with relatively low values of SLS, whereas the appearance of martensite nuclei are registered at $SLS \leq 20 \mu v$ due to the relatively low amplitude and the energy of the mechanical waves generated by the sources of internal stresses formed around the nuclei of martensite.

6. The results of the tensile testing sample made of 12X18H10T steel, welded from two halves using a laser welding fiber laser, show that in the range of loads from 200 to 700 MPa and weld seam internal stress at the half of the sample, which is located behind the weld relative to the active capture of the testing machine.

7. The methodology of complex research using the methods of scanning contact potentiometry and diffraction of thermal neutrons at the pulsed fast reactor IBR-2 in FLNP JINR in Dubna allows you to decide on a high technical level, as the fundamental material science challenges and developing tools and techniques electro-physical diagnostics and nondestructive testing.

References

- [1] V.I. Surin, A.A. Abu Ghazal, E.V. Voloshin, E.Y. Telnov, D.O. Titovets, «Device's for measuring contact surface stress»// Journal of Advanced Research in Technical Science, -North Charleston, USA: SRC MS, CreateSpace.- 2017.- Issue 6. pp. 48-54.
- [2] G.D. Bokuchava, V.L. Aksenov, A.M. Balagurov, V.V. Zhuravlev, E.S. Kuzmin, A.P. Bulkin, V.A. Kudryashev, V.A. Trounov, "Neutron Fourier diffractometer FSD for internal stress analysis: first results", Applied Physics A: Materials Science & Processing, v.74 [Suppl], 2002, pp s86-s88. <http://dx.doi.org/10.1007/s003390201750>
- [3] A.M. Balagurov, G.D. Bokuchava, E.S. Kuzmin, A.V. Tamonov, V.V. Zhuk, "Neutron RTOF diffractometer FSD for residual stress investigation", Zeitschrift für Kristallographie, Supplement Issue No. 23, 2006, pp. 217-222. <http://dx.doi.org/10.1524/9783486992526-038>
- [4] G.D. Bokuchava, "Materials microstructure characterization using high resolution time-of-flight neutron diffraction", Romanian Journal of Physics, 2016, Vol. 61, No. 5-6, pp. 903-925. http://www.nipne.ro/rjp/2016_61_5-6/0903_0925.pdf
- [5] A.M. Balagurov, I.A. Bobrikov, G.D. Bokuchava, V.V. Zhuravlev, V.G. Simkin, "Correlation Fourier Diffractometry: 20 Years of Experience at the IBR-2 Reactor", Physics of Particles and Nuclei, 2015, Vol. 46, Issue 3, pp. 249-276.

- <http://doi.org/10.1134/S1063779615030041>
- [6] G.D. Bokuchava, I.V. Papushkin, A.V. Tamonov, A.A. Kruglov, "Residual stress measurements by neutron diffraction at the IBR-2 pulsed reactor", *Romanian Journal of Physics*, 2016, Vol. 61, No. 3-4, pp. 491-505. http://www.nipne.ro/rjp/2016_61_3-4/0491_0505.pdf
- [7] М.А. Штремель. Прочность сплавов. Часть II. Деформация. – М.: МИСИС, 1997. – 527 с.
- [8] V. I. Surin, A. A. Morozov, P. V. Potapov, A. E. Batukhtin. Deformation activity of the metal surface as a factor influencing the work function of electrons// Scientific session MEPhI-2010. Abstract reports. In 3 volumes. Volume 2. Nanophysics and nanotechnology. Fundamental problems of science. Moscow: MEPhI, 2010. – 344 p. (p. 88).
- [9] V. I. Surin, A.V. Osintsev, V. I. Polish, P. S. Jumaev. Modeling of surface stresses in tension steel samples using the method of scanning contact potentiometry// "Information technologies in design and production", Moscow: FGUP VIMI, 2017, № 2(166).pp.42-49.
- [10] H.M. Rietveld, "A profile refinement method for nuclear and magnetic structures", *Journal of Applied Crystallography*, Vol. 2, 1969, pp. 65-71. <http://dx.doi.org/10.1107/S0021889869006558>